Article

Synthesis of Hierarchical Porous Carbon in Molten Salt and Its Application for Dye Adsorption

Saisai Li [1], Haijun Zhang [1],* , **Shiya Hu [1], Jie Liu [1], Qing Zhu [1] and Shaowei Zhang [2],***

[1]   The State Key Laboratory of Refractories and Metallurgy, Wuhan University of Science and Technology, Wuhan 430081, China
[2]   College of Engineering, Mathematics and Physical Sciences, University of Exeter, Exeter EX4 4QF, UK
*   Correspondence: zhanghaijun@wust.edu.cn (H.Z.); s.zhang@exeter.ac.uk (S.Z.)

check for updates

Abstract: Hierarchical porous carbon was successfully synthesized from glucose in a molten salt at 800 °C for 2 h. It was amorphous and contained numerous oxygen containing functional groups on its surface. The porous carbon with 1.0 wt% $Fe(NO_3)_3 \cdot 9H_2O$ oxidizing agent showed the highest specific surface area of 1078 m^2/g, and the largest pore volume of 0.636 cm^3/g, among all of the samples. Raman and TEM results revealed that it had more defects and pores than other as-prepared carbon materials. The adsorption capacities of as-prepared porous carbon for methylene blue (MB) and methyl orange (MO) were 506.8 mg/g and 683.8 mg/g, respectively. The adsorption isotherms fit the Langmuir model and the adsorption kinetics followed the pseudo-second-order kinetic model.

Keywords: hierarchically porous carbon; molten salt method; $Fe(NO_3)_3 \cdot 9H_2O$; dye adsorption

1. Introduction

Dyes have long been used in plastic, paper, leather, textile, and other industrial sectors. Wastewaters discharged from these industrial sectors often contain a certain amount of dyes, especially water-soluble organic dyes, due to their low biodegradability [1–3]. The conventional biological treatment processes fail to effectively treat these dye wastewaters, due to which, several physical or chemical processes, including osmosis [4], electro flotation [5], chemical oxidation [6], ion exchange [7], and filtration [8], have been developed in recent years. Unfortunately, these processes are not economically-viable and are still not sufficiently effective for treating a wide range of dye wastewaters [9]. Physical adsorption has become the most popular method so far for removing dyes from wastewaters, owing to its low cost, high efficiency, easy operation, diversity in adsorbents, and high stability towards the adsorbents.

Porous carbon materials have been widely applied for removing dyes and other organic and inorganic pollutants from drinking water due to their high specific surface area [10–12]. In particular, those with hierarchical porosities (micro-/meso-/macropore) exhibit enhanced dye adsorption performance. This is because that the hierarchical pore structures can provide various functions: Micropores provide high surface area and large adsorption capacity, mesopores facilitate dye transporting, and macropores act as reservoirs for dye molecules.

Several techniques, mainly physical or chemical activation combined with templating, have been used to synthesize hierarchical porous carbon materials [13–15]. However, they exhibited some disadvantages, such as high carbonization temperature, multiple steps, low carbon yield, vessel corrosion, and environmental pollution. Recently, molten salt synthesis methods have become applicable to the preparation of a wide range of nanomaterials, including binary, ternary/multinary oxides [16–25], hydroxide [26], non-oxides [27], and porous carbon materials [28–31]. For example, Liu et al. synthesized porous carbon and carbon sheets in molten LiCl/KCl containing different oxysalts (such as $Fe(NO_3)_3 \cdot 9H_2O$, $KClO_3$, and K_2CO_3), which facilitated pore formation in the final porous

carbon [32]. Deng et al. prepared nitrogen-doped hierarchically porous carbon materials with high specific surface area in molten $ZnCl_2$ [33]. Despite these studies, there have been few studies on the preparation of porous carbon with high specific surface area by using a combined activator, $ZnCl_2$ and $Fe(NO_3)_3\cdot9H_2O$.

In this work, hierarchical porous carbon was synthesized in $ZnCl_2$-KCl molten salt using a low-cost and eco-friendly glucose carbon source and an $Fe(NO_3)_3\cdot9H_2O$ oxidizing agent. The effects of additional amounts of $Fe(NO_3)_3\cdot9H_2O$ on the specific surface area of as-prepared samples were investigated, as were their adsorption capacities for methylene blue (MB) and methyl orange (MO).

2. Materials and Methods

2.1. Raw Materials and Sample Preparation

The main starting materials included: Glucose ($C_6H_{12}O_6\cdot H_2O$, AR; Bodi chem. Co. Ltd. Tianjin, China), zinc chloride ($ZnCl_2$, AR; Sinopharm chem. Co. Ltd. Shanghai, China), potassium chloride (KCl, AR; Sinopharm chem. Co. Ltd. Shanghai, China), commercial ferric nitrate ($Fe(NO_3)_3\cdot9H_2O$, 99.0%, Lia Chemical Co., Ltd. Wuhan, China), commercial ferric chloride ($FeCl_3\cdot6H_2O$, 99.0%, Lia Chemical Co., Ltd. Wuhan, China), zinc nitrate ($Zn(NO_3)_2$, AR; Sinopharm chem. Co. Ltd. Shanghai, China), methylene blue trihydrate ($C_{16}H_{18}ClN_3S\cdot3H_2O$, Sinopharm chem. Co., Lth. Shanghai, China), and methyl orange ($C_{14}H_{14}N_3SO_3Na$, Sinopharm chem. Co., Lth. Shanghai, China).

In a typical preparation process, 2 g glucose and different amounts of $Fe(NO_3)_3\cdot9H_2O$ (0–2.0 wt% Fe of carbon amount, the samples are referred to as 0 Fe, 0.5 Fe, 1.0 Fe, 1.5 Fe, and 2.0 Fe, respectively) were milled together and further combined with 20 g of KCl and $ZnCl_2$ (in the weight ratio of 1:2. The eutectic point of the binary salt is 234 °C.). The mixed powder was contained in an alumina crucible and heated at 2 °C/min to 800 °C and soaked for 2 h in an alumina tube furnace protected by flowing Ar (99.999 vol% pure). The reacted sample was subjected to repeat water-washing before being oven-dried for 12 h at 80 °C.

2.2. Adsorption Test

Adsorption processes were investigated using MB and MO. Typically, 20 mg of as-prepared sample (porous carbon) powder was added into 50 mL MB aqueous solution with a concentration ranging from 0 to 500 mg/L. The suspension was then homogenized for 30 min at 25 °C using a magnetic stirrer. After centrifugation, the solution part was examined using a UV-visible spectrophotometer.

To study the adsorption kinetics, 60 mg of as-prepared porous carbon were added to 150 mL aqueous dye solution (100 mg/L) in a beaker. The suspension was stirred using a magnetic stirrer. After a certain time period, 5 ml of the solution was taken and centrifuged for UV-vis examination. The maximum adsorption wavelengths of 665 nm and 464 nm, in the cases of MB and MO, were used respectively for calculation.

The equilibrium adsorption amount of the porous carbon materials was determined based on the following equation:

$$q_e = \frac{(c_0 - c_e)v}{m} \tag{1}$$

where q_e (mg/g) is the equilibrium adsorption amount, c_0 (mg/L) is the initial concentration of dye solution, c_e (mg/L) is the equilibrium concentration of dye solution, v (L) is the volume of dye solution, and m (g) is the mass of porous carbon.

2.3. Characterization

Powder X-ray diffraction (XRD) analysis was carried out using a Philips X'Pert PRO diffractometer (Xpertpro, PHILIPS, Hillsboro, The Netherlands) at 40 mA and 40 kV and with a Cu Kα radiation (λ = 0.1542 nm). The scan range was between 10° and 90° (2θ) at 40 mA and 40 kV and the scan rate was 2°/min with a step size of 0.05°. Microstructure and phase morphologies of as-prepared samples were

examined by using a field-emission scanning electron microscope (FE-SEM; Nova400NanoSEM, 15 kV, Philips, Amsterdam, The Netherlands) and a transmission electron microscope (TEM) JEM-2100UHRSTEM, 200 kV (JEOL, Tokyo, Japan) along with an energy dispersive spectrometer (EDS) Penta FET X-3 Si (Li) (EDS, IET 200, Oxford, UK). The specific surface area of as-prepared samples was calculated based on Brunauere Emmette Teller (BET) nitrogen adsorption/desorption analysis carried out using a gas sorption analyzer Autosorb-1-MP/LP (Quantachrome, Boynton Beach, FL, USA). Functional groups on the surface of a sample were identified by Fourier Transform Infrared Spectroscopy (FTIR) VERTEX 70 (Bruker, Karlsruhe, Germany). The adsorption of MB or MO was examined by Ultraviolet–visible spectroscopy UV-2550 (Shimadzu Corporation, Kyoto, Japan). Raman spectra were recorded using a Horiba Jobin-Yvon Labram-HR800 Raman spectrometer (Raman, Paris, France) with an excitation wavelength of 532 nm.

3. Results and Discussion

3.1. Microstructural Characterization of As-Prepared Porous Carbon

Powder X-ray diffraction patterns of samples resultant from 2 h firing in molten salt at 800 °C are shown in Figure 1a, revealing a broad diffraction peak in each case, centered at approximately 26° and corresponding to the (002) lattice plane of graphite, and indicating the amorphous nature of the carbon formed in the samples. Apart from the amorphous carbon, Fe_2O_3 and Fe_3O_4 were identified in the samples using $Fe(NO_3)_3 \cdot 9H_2O$, suggesting the decomposition of $Fe(NO_3)_3 \cdot 9H_2O$ into Fe_2O_3 firstly and then some Fe_2O_3 became Fe_3O_4 by reductive carbon coming from glucose upon firing [34,35]. The obtained lattice parameter values for Fe_2O_3 were, respectively, $a = 13.21$ Å, $b = 9.78$ Å, and $c = 8.37$ Å, and $a = 6.21$ Å, $b = 5.89$ Å and $c = 14.77$ Å for Fe_3O_4. Fourier transform infrared spectroscopy were used to identify functional groups in as-prepared carbons with various amounts of $Fe(NO_3)_3 \cdot 9H_2O$ (Figure 1b). The main bands at 1316 and 1617 cm^{-1} were attributed to the C=C stretching vibration, and the other two bands at 3470 and 1380 cm^{-1} corresponded to the O–H (hydroxyl or carboxyl) stretching vibration and the C–OH stretching vibration, respectively, and this later verified the existence of aldehyde. The above observations indicated the existence of oxygen containing functional groups on the carbon formed in as-prepared samples, which favored the adsorption of the dyes [36].
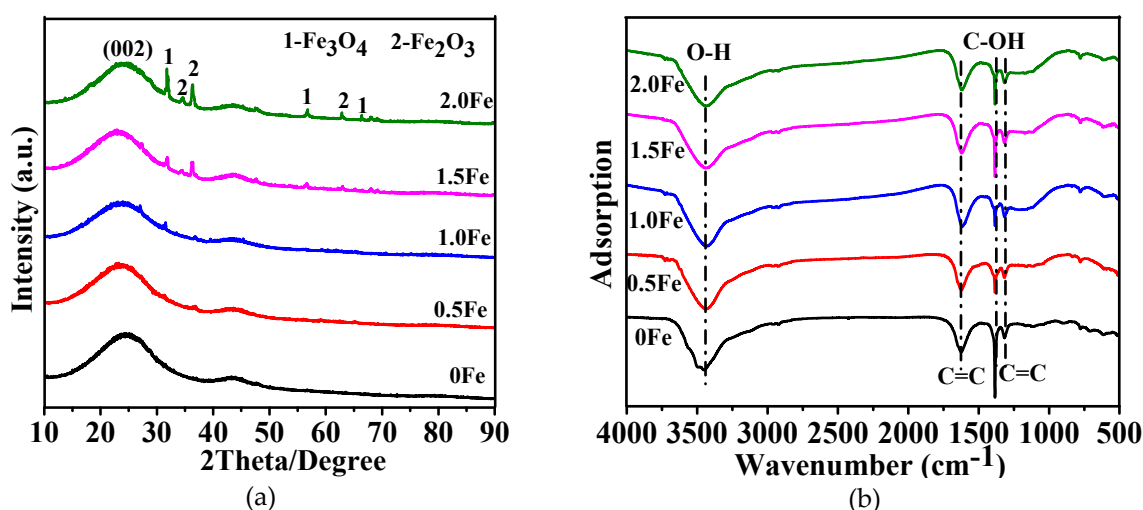
Figure 1. (**a**) Powder X-ray diffraction (XRD) pattern and (**b**) Fourier transform infrared spectroscopy (FTIR) of as-prepared samples with various amounts of $Fe(NO_3)_3 \cdot 9H_2O$. (ICDD: 00-016-0653 (Fe_2O_3) and 01-076-0956 (Fe_3O_4)).

Scanning electron microscope images of as-prepared carbon samples resulting from 2 h firing at 800 °C in the molten salt with various amounts of $Fe(NO_3)_3 \cdot 9H_2O$ are shown in Figure 2, and reveal the formation of irregular carbon particles and carbon sheets. With increasing Fe content, the morphology of the carbon particles changed very little. The carbon particles resulted from the decomposition of glucose and the nucleation of intermediates and their subsequent growth during carbonization, whereas the carbon sheets were formed via the merging and growing of carbon particles facilitated by highly reactive lithium, potassium, and chloride ions in the molten salt medium [37,38].
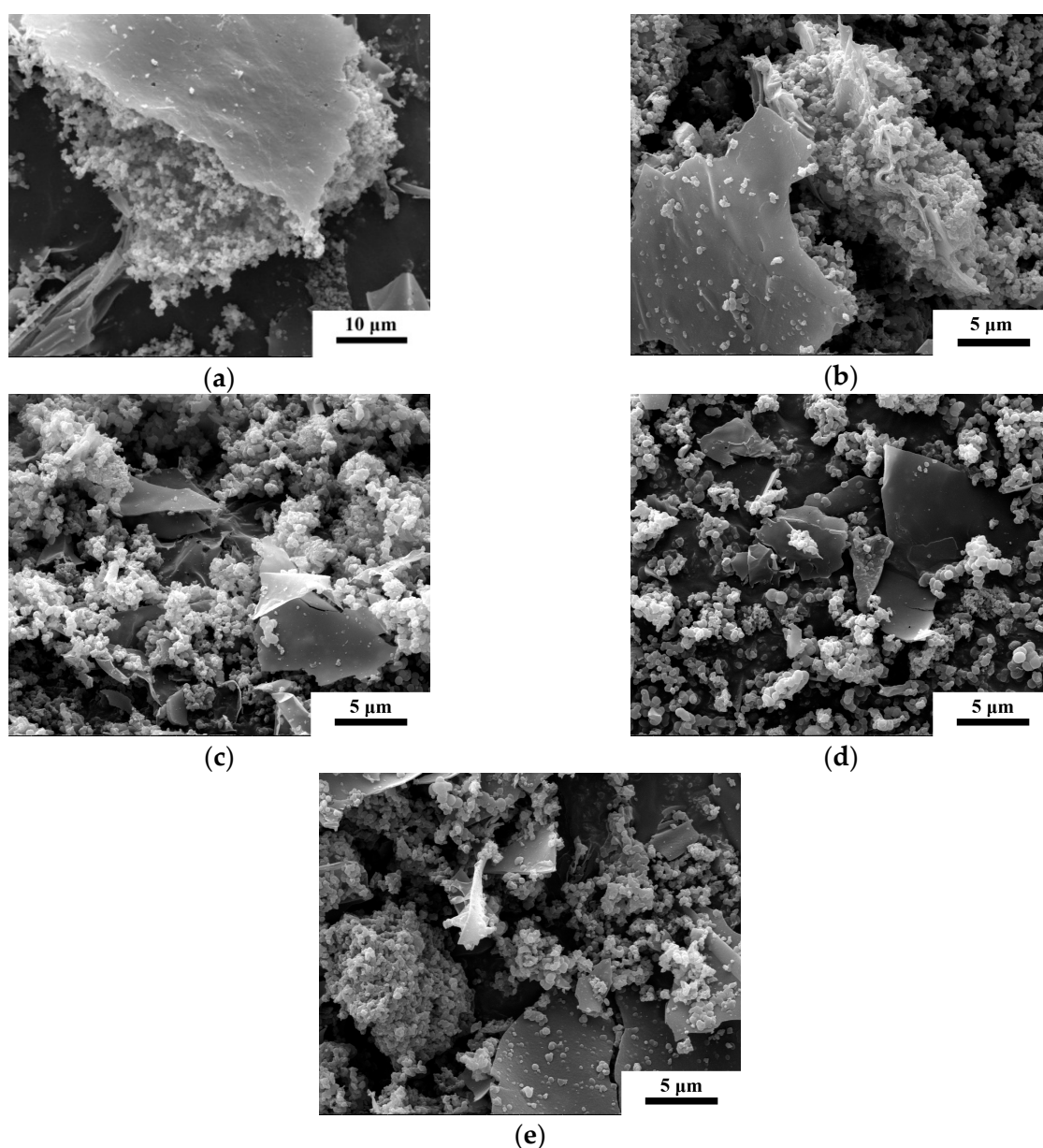
Figure 2. Scanning electron microscope (SEM) images of as-prepared samples whose XRD patterns are shown in Figure 1a. (**a**) 0 Fe, (**b**) 0.5 Fe, (**c**) 1.0 Fe, (**d**) 1.5 Fe, (**e**) 2.0 Fe.

N_2 adsorption–desorption isotherms of as-prepared carbon samples, along with the derived pore size distributions are presented in Figure 3. Similar type I isotherms were seen in all cases, and the adsorption amounts within different relative pressure ranges reflected different pore structures (micropores (P/P_0 between 0–0.1), mesopores (P/P_0 between 0.1–0.8), and macroporous (P/P_0 between 0.8–1.0) [39,40]. Therefore, the N_2 sorption profiles evidently reveal that the as-prepared carbon

materials possessed a hierarchical micro-/mesoporous structure. From Figure 3a, it can be seen that the sample with 1.0 wt% Fe showed the maximum adsorption volume, indicating it has the largest specific surface area. Figure 3b shows the pore size distribution curves derived from the desorption isotherms using the Barret–Joner–Halenda (BJH) method, which reveal the formation of mainly micro- and meso-porosities in as-prepared carbon materials. The porosity parameters of as-prepared porous carbon materials are listed in Table 1. As can be seen from Table 1, the BET specific surface areas of all of the samples with $Fe(NO_3)_3 \cdot 9H_2O$ increased compared to the sample without $Fe(NO_3)_3 \cdot 9H_2O$, and upon increasing the amount of $Fe(NO_3)_3 \cdot 9H_2O$ to 1.0 wt%, the sample showed the highest BET specific surface area of 1078 m^2/g and the highest pore volume of 0.636 cm^3/g. Furthermore, the mesoporous volume percent reached up to 60% with increasing the Fe amount to 1.0–1.5 wt%, which was probably mainly due to the decomposition of $Fe(NO_3)_3 \cdot 9H_2O$ during carbonization [41].
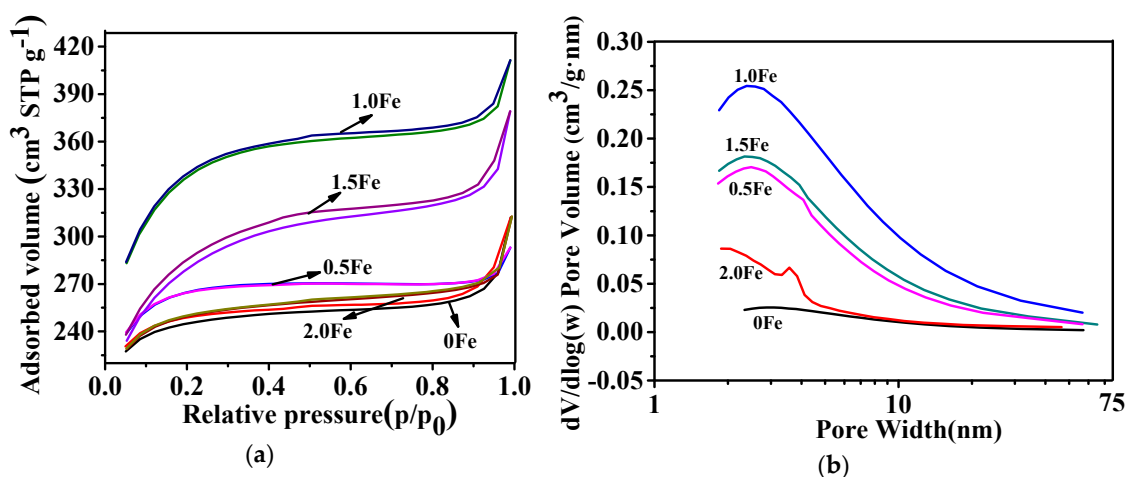

Figure 3. (**a**) N_2 adsorption–desorption isotherms and (**b**) pore size distribution curves of porous carbon prepared at 800 °C for 2 h with various amounts of Fe.

Table 1. Porosity parameters of as-prepared porous carbon prepared with various amounts of Fe.

| Sample	S_{BET} (m^2/g)	V_{total} (cm^3/g)	V_{meso} (cm^3/g)	V_{meso}/V_{total} (%)
0 Fe	753	0.453	0.141	31.1
0.5 Fe	817	0.483	0.173	35.8
1.0 Fe	1078	0.636	0.375	59.0
1.5 Fe	903	0.586	0.357	60.9
2.0 Fe	767	0.484	0.183	37.8

Figure 4 presents Raman spectra of porous carbon materials prepared at 800 °C for 2 h with various amounts of Fe. Two main peaks at 1350 and 1590 cm^{-1} were respectively assigned to the D band and G band [42]. With the increase of the Fe amount, the value of I_D/I_G increased initially and then decreased, demonstrating the existence of many defects in the as-prepared porous carbon.
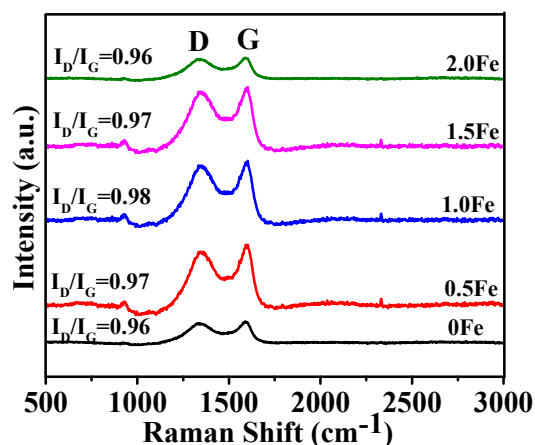
Figure 4. Raman spectra of porous carbon prepared at 800 °C for 2 h with various amounts of Fe.

Based on the above test results, it can be concluded that addition of 1.0 wt% $Fe(NO_3)_3 \cdot 9H_2O$, resulted in the largest specific surface area. In order to compare and further reveal the effectiveness of $Fe(NO_3)_3 \cdot 9H_2O$, samples using respectively $FeCl_3 \cdot 6H_2O$ and $Zn(NO_3)_2$ as oxidizing agents were also prepared under similar processing conditions to those in the case of using 1.0 wt% $Fe(NO_3)_3 \cdot 9H_2O$. Amorphous carbon was also formed in these two cases (Figure S1). For the sample with added $FeCl_3 \cdot 6H_2O$, one peak at about 36.2° appeared, which was corresponded to Fe_3O_4. As shown in Figure S2, porous carbons prepared using $FeCl_3$ and $Zn(NO_3)_2$ as oxidizing agents were mainly comprised of carbon particles. Different from the case of using $Fe(NO_3)_3 \cdot 9H_2O$, carbon sheets were only occasionally seen. FTIR identified the existence of some oxygen containing functional groups and C–H groups on the surface of as-prepared porous carbon (Figure S3). The specific surface areas of the samples prepared with $FeCl_3$ and $Zn(NO_3)_2$ were 534 and 654 m^2/g, respectively (Figure S4), which are even lower than that of the sample prepared without using any oxidizing agents (Table 1), indicating that neither $FeCl_3$ nor $Zn(NO_3)_2$ was useful for increasing the specific surface area. The sample with $Zn(NO_3)_2$ had a higher surface area than in the case of using $FeCl_3$, which was attributed to the oxidizability of $Zn(NO_3)_2$. The samples prepared with $Fe(NO_3)_3 \cdot 9H_2O$ showed the highest surface area, since $Fe(NO_3)_3 \cdot 9H_2O$ can act as an effective oxidizing agent during carbonization [43]. It reacts with glucose and releases some gaseous phases, such as NO_x, CO, and CO_2, facilitating the formation of micro/mesopores [41]. Comparison of the Raman results (Figure S5 and Figure 4) also reveals that the samples with $Fe(NO_3)_3 \cdot 9H_2O$ had a higher I_D/I_G value, suggesting the existence of more defects in them.

In order to further reveal the porous structures of the as-prepared carbon materials, Figure 5, as an example, shows TEM images and EDS results of the sample prepared with 1.0 wt% Fe. As seen from Figure 5a,b, the as-prepared carbon contained a large number of mesopores, which were consistent with the BET results (Figure 3). EDS of the selected region in Figure 5a indicated that the sample was mainly composed of C, Fe, and O elements.
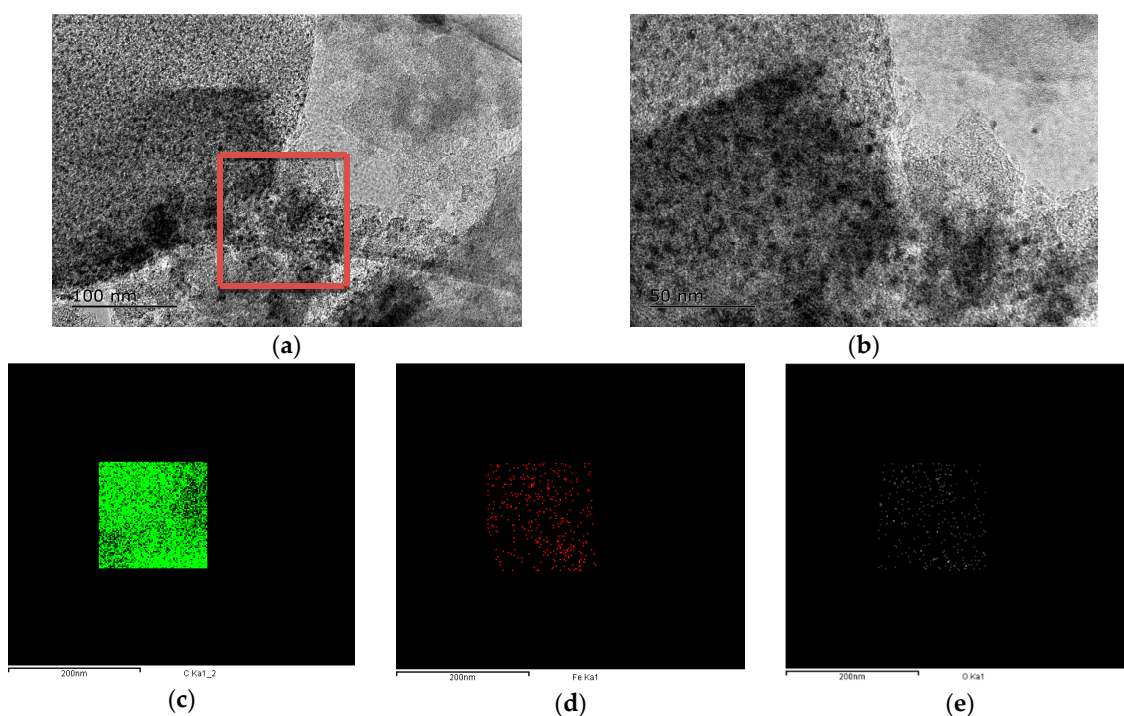
Figure 5. Transmission electron microscope (TEM) and energy dispersive spectrometer (EDS) results of the sample prepared with 1.0 wt% Fe. (**a**) Low-resolution image, (**b**) high-resolution image, (**c**) mapping scan of C in red box, (**d**) mapping scan of Fe in red box, and (**e**) mapping scan of O in red box.

3.2. Adsorption Performance of As-Prepared Porous Carbon for Methylene Blue and Methyl Orange

The adsorption behaviors of porous carbon materials prepared with various amounts of Fe (Figures 1–5) were also examined using MB and MO as adsorbates, and the adsorption isotherms were simulated using the Langmuir and Freundlich models expressed as follows:

$$\text{Langmuir isotherm}: \quad q_e = \frac{Q_0{}^b c_e}{1 + c_e^{\frac{1}{n}}} \tag{2}$$

$$\text{Freundlich isotherm}: \quad q_e = k_F c_e^{\frac{1}{n}} \tag{3}$$

where q_e (mg/g) is the equilibrium adsorption amount, Q_0 (mg/g) is the maximum adsorption amount, b (L/mg) is the constant term related to the energy of adsorption, c_e (mg/L) is the equilibrium concentration of dye solution, and k_F and n are the Freundlich constants.

The calculated adsorption parameters and correlation coefficients (R^2) (Tables 2 and 3) suggest that the Langmuir model fits the data better than the Freundlich model. The maximum monolayer adsorption capacity (Q_0) of the as-prepared porous carbon (1.0 Fe) for MB and MO were calculated to be 506.8 and 683.8 mg/g, respectively, which was mainly attributed to the much larger specific surface area of the hierarchical porous carbon materials and the oxygen containing functional groups existing on their surfaces. Table 4 compares the adsorption capacity for dyes of hierarchical porous carbon materials and other adsorbents. The high adsorption capacity of hierarchical porous carbon materials prepared in this work indicates their feasibility in dye removal.

Table 2. Kinetics parameters calculated on the basis of Equations (2) and (3) for methylene blue (MB) adsorption of porous carbon prepared with various amounts of Fe.

Sample	Dyes	Langmuir			Freundlich			Pseudo-First-Order			Pseudo-Second-Order		
		Q_0	B	R^2	K_F	N	R^2	Q_e	K_1	R^2	Q_e	K_2	R^2
0 Fe		188.4	0.031	0.83	1.6	1.15	0.91	124.8	0.50	0.995	142.9	0.016	0.999
0.5 Fe		412	0.012	0.94	1.5	1.01	0.95	240	0.59	0.992	250	0.012	0.999
1.0 Fe	MB	506.8	0.009	0.96	1.4	0.99	0.96	274.7	0.59	0.995	333.3	0.009	0.998
1.5 Fe		442.5	0.011	0.95	1.4	1.0	0.95	260.9	0.41	0.993	277.8	0.005	0.999
2.0 Fe		194	0.029	0.84	1.6	1.2	0.91	127	0.50	0.996	142.9	0.012	0.998

Table 3. Kinetics parameters calculated on the basis of Equations (2) and (3) for methyl orange (MO) adsorption of porous carbon prepared with various amounts of Fe.

Sample	Dyes	Langmuir			Freundlich			Pseudo-First-Order			Pseudo-Second-Order		
		Q_0	B	R^2	K_F	N	R^2	Q_e	K_1	R^2	Q_e	K_2	R^2
0 Fe		249.5	0.020	0.95	1.7	1.16	0.91	161.5	0.58	0.998	166.7	0.016	0.999
0.5 Fe		559	0.008	0.98	1.5	1.02	0.95	311.9	0.50	0.995	333.3	0.005	0.999
1.0 Fe	MO	683.8	0.007	0.96	1.1	0.99	0.94	370.7	0.60	0.995	379	0.007	0.998
1.5 Fe		521	0.007	0.96	1.4	1.0	0.95	334.1	0.56	0.993	344.8	0.006	0.999
2.0 Fe		254	0.020	0.98	1.8	1.2	0.90	166.8	0.51	0.996	172.4	0.013	0.999

Table 4. Comparison of dye adsorption capacity of hierarchical porous carbon prepared in this work and other adsorbents reported in the literature.

Adsorbent	Dyes	T (°C)	BET (m^2/g)	Qm (mg/g)	Reference
Mesoporous activated carbon	MB	30	1135	359	[44]
Activated carbon	MB	30~50	1940	434.78	[45]
Activated carbon	MB	30~50	1060	102.04	[3]
Activated carbon	MG	25~50	1000	149	[46]
Porous carbon	RB	-	2721	479	[47]
Hierarchical porous carbon materials	MB/DB	25	1913	1585.7/438.6	[48]
Hierarchical porous carbon materials	MO	25	1338.9	598.8	[49]
Hierarchical porous carbon materials	MB/MO	25	1078	506.8/683.8	This work

BET: Brunauere Emmette Teller, RB: Rhodamine B, DB: Direct black 38, MG: Malachite green.

The following pseudo-first-order and pseudo-second-order kinetic models [1] were also used to assist understanding the relevant adsorption mechanism:

$$\text{Pseudo-first-order model}: \quad q_t = q_e(1 - e^{-k_1 t}) \tag{4}$$

$$\text{Pseudo-second-order model}: \quad \frac{t}{q_t} = \frac{1}{\kappa_2 q_e^2} + \frac{t}{q_e} \tag{5}$$

where q_t (mg/g) is the adsorption amount at time t, k_1 and k_2 (g·mg^{-1}·min^{-1}) are respectively the pseudo-first-order and pseudo-second-order rate constants.

As indicated by the results listed in Tables 2 and 3, the pseudo-second-order model shows a good linearity, with correlation coefficients (R^2) ≥ 0.99, suggesting that the adsorption kinetics of as-prepared porous carbon follow this model (Figure 6).
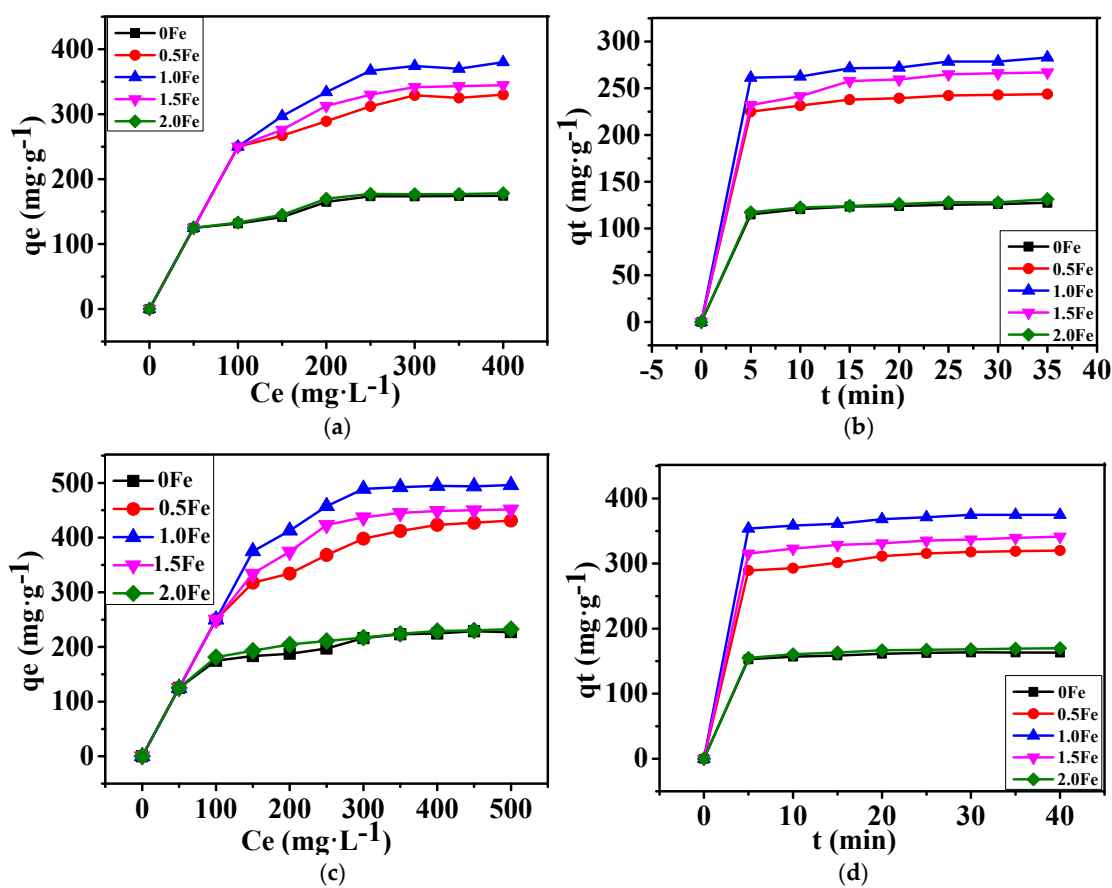
Figure 6. Adsorption isotherms and kinetics of porous carbon prepared at 800 °C for 2 h with various amounts of Fe. (**a**) Adsorption isotherms of MB, (**b**) adsorption kinetics of MB, (**c**) adsorption isotherms of MO, (**d**) adsorption kinetics of MO.

4. Conclusions

A simple molten salt method was used to synthesize hierarchical porous carbon at 800 °C for 2 h. Glucose and $ZnCl_2$-KCl were used as the carbon source and reaction medium, respectively. Numerous oxygen containing functional groups existed on the surface of the as-prepared porous carbon. The porous carbon prepared with 1.0 wt% $Fe(NO_3)_3 \cdot 9H_2O$ addition showed the highest specific surface area of 1078 m^2/g and the largest pore volume of 0.636 cm^3/g, which were attributed to $Fe(NO_3)_3 \cdot 9H_2O$ acting as an oxidizing agent during carbonization, favoring the formation of micro/mesopores. The adsorption capacities of as-prepared hierarchical porous carbon for methylene blue and methyl orange were respectively 506.8 mg/g and 683.8 mg/g. The adsorption isotherms fit the Langmuir model and the adsorption kinetics followed the pseudo-second-order kinetic model.

References

1. Siyasukh, A.; Chimupala, Y.; Tonanon, N. Preparation of magnetic hierarchical porous carbon spheres with graphitic features for high methyl orange adsorption capacity. *Carbon* **2018**, *134*, 207–221. [CrossRef]

2. Yagub, M.T.; Sen, T.K.; Afroze, S. Dye and its removal from aqueous solution by adsorption. *Adv. Colloid Interfac.* **2014**, *209*, 172–184. [CrossRef]

3. Başar, C.A. Applicability of the various adsorption models of three dyes adsorption onto activated carbon prepared waste apricot. *J. Hazard Mater.* **2006**, *135*, 232–241. [CrossRef]

4. Öner, Ş.G.; Kabay, N.; Güler, E. A comparative study for the removal of boron and silica from geothermal water by cross-flow flat sheet reverse osmosis method. *Desalination* **2011**, *283*, 10–15. [CrossRef]

5. Murugananthan, M.; Raju, G.B.; Prabhakar, S. Separation of pollutants from tannery effluents by electro flotation. *Sep. Purif. Technol.* **2004**, *40*, 69–75. [CrossRef]

6. Dutta, K.; Mukhopadhyay, S.; Bhattacharjee, S. Chemical oxidation of methylene blue using a Fenton-like reaction. *J. Hazard Mater.* **2001**, *84*, 57–71. [CrossRef]

7. Vilensky, M.Y.; Berkowitz, B.; Warshawsky, A. In Situ remediation of groundwater contaminated by heavy- and transition-metal ions by selective ion-exchange methods. *Environ. Sci. Technol.* **2002**, *36*, 1851–1855. [CrossRef]

8. Huq, A.; Xu, B.; Chowdhury, M.A. A simple filtration method to remove plankton-associated *Vibrio cholerae* in raw water supplies in developing countries. *Appl. Environ. Microb.* **1996**, *62*, 2508–2512.

9. SariciÖzdemir, Ç.; Önal, Y. Study to observe the applicability of the adsorption isotherms used for the adsorption of medicine organics onto activated carbon. *Part. Sci. Technol.* **2018**, *36*, 254–261. [CrossRef]

10. Önal, Y.; Akmil-Başar, C.; Sarıcı-Özdemir, Ç. Elucidation of the naproxen sodium adsorption onto activated carbon prepared from waste apricot: Kinetic, equilibrium and thermodynamic characterization. *J. Hazard Mater.* **2007**, *148*, 727–734. [CrossRef]

11. Önal, Y.; Akmil-Başar, C.; Eren, D. Adsorption kinetics of malachite green onto activated carbon prepared from Tunçbilek lignite. *J. Hazard Mater.* **2006**, *128*, 150–157. [CrossRef]

12. Gu, L.; Zhu, N.; Guo, H. Adsorption and Fenton-like degradation of naphthalene dye intermediate on sewage sludge derived porous carbon. *J. Hazard Mater.* **2013**, *246–247*, 145–153. [CrossRef]

13. Lei, Z.; Xiao, Y.; Dang, L. Graphitized carbon with hierarchical mesoporous structure templated from colloidal silica particles. *Microporous Mesoporous Mater.* **2008**, *109*, 109–117. [CrossRef]

14. Gorka, J.; Zawislak, A.; Choma, J.; Jaroniec, M. KOH activation of mesoporous carbons obtained by soft-templating. *Carbon* **2008**, *46*, 1159–1161. [CrossRef]

15. Wang, X.; Wang, H.; Dai, Q. Preparation of novel porous carbon spheres from corn starch. *Colloid Surface A* **2009**, *346*, 213–215. [CrossRef]

16. Reddy, M.V.; Yu, C.; Jiahuan, F. Molten salt synthesis and energy storage studies on $CuCo_2O_4$ and $CuO\cdot Co_3O_4$. *RSC Adv.* **2012**, *2*, 9619–9625. [CrossRef]

17. Reddy, M.V.; Beichen, Z.; Nichollette, L.J.E.; Kaimeng, Z.; Chowdari, B.V.R. Molten salt synthesis and its electrochemical characterization of Co_3O_4 for lithium batteries. *Electrochem. Solid State Lett.* **2011**, *14*, 79–82. [CrossRef]

18. Reddy, M.V.; Cherian, C.T.; Ramanathan, K. Molten synthesis of $ZnO\cdot Fe_3O_4$ and Fe_2O_3 and its electrochemical performance. *Electrochimica Acta* **2014**, *118*, 75–80. [CrossRef]

19. Reddy, M.V.; Teoh, X.W.V.; Nguyen, T.B. Effect of 0.5 M $NaNO_3$: 0.5 M KNO_3 and 0.88 M $LiNO_3$: 0.12 M LiCl molten salts. and heat treatment on electrochemical properties of TiO_2. *J. Electrochem. Soc.* **2012**, *159*, 762–769. [CrossRef]

20. Nithyadharseni, P.; Reddy, M.V.; Ozoemena, K.I. Low temperature molten salt synthesis of $Y_2Sn_2O_7$ anode material for lithium ion batteries. *Electrochim. Acta* **2015**, *182*, 1060–1069. [CrossRef]

21. Reddy, M.V.; Tung, B.D.; Yang, L. Molten salt method of preparation and cathodic studies on layered-cathode materials $Li(Co_{0.7}Ni_{0.3})O_2$ and $Li(Ni_{0.7}Co_{0.3})O_2$ for Li-ion batteries. *J. Power Sources* **2013**, *225*, 374–381. [CrossRef]

22. Reddy, M.V.; Beichen, Z.; Loh, K.P. Facile synthesis of Co_3O_4 by molten salt method and its Li-storage performance. *CrystEngComm* **2013**, *15*, 3568–3574. [CrossRef]

23. Tan, K.S.; Reddy, M.V.; Rao, G.V. High-performance $LiCoO_2$ by molten salt ($LiNO_3$: LiCl) synthesis for Li-ion batteries. *J. Power Sources* **2015**, *147*, 241–248. [CrossRef]

24. Reddy, M.V.; Rao, G.V.S.; Chowdari, B.V.R. Synthesis by molten salt and cathodic properties of $Li(Ni_{1/3}Co_{1/3}Mn_{1/3})O_2$. *J. Power Sources* **2006**, *159*, 263–267. [CrossRef]

25. Reddy, M.V.; Rao, G.V.S.; Chowdari, B.V.R. Synthesis and electrochemical studies of the 4V cathode, $Li(Ni_{2/3}Mn_{1/3})O_2$. *J. Power Sources* **2006**, *160*, 1369–1374. [CrossRef]

26. Hudry, D.; Rakhmatullin, A.; Bessada, C. Reactivity of $NH_4H_2PO_4$ toward $LaCl_3$ in LiCl-KCl melt flux step by step formation of monazite-Like $LaPO_4$. *Inorg. Chem.* **2009**, *48*, 7141–7150. [CrossRef]

27. Portehault, D.; Devi, S.; Beaunier, P. A general solution route toward metal boride nanocrystals. *Angew. Chem. Int. Ed.* **2011**, *123*, 3320–3323. [CrossRef]

28. Ye, L.; Zhao, L.; Liang, F. Facile synthesis of hexagonal boron nitride nanoplates via molten-salt-mediated magnesiothermic reduction. *Ceram. Int.* **2015**, *41*, 14941–14948. [CrossRef]

29. Liang, F.; Tian, L.; Zhang, H. Low temperature synthesis of $LiSi_2N_3$ nanobelts via molten salt nitridation and their photoluminescence properties. *RSC Adv.* **2016**, *6*, 68615–68618. [CrossRef]

30. Liu, J.; Huang, Z.; Huo, C. Low-temperature rapid synthesis of rod-like ZrB_2 powders by molten-salt and microwave Co-assisted carbothermal reduction. *J. Am. Ceram. Soc.* **2016**, *99*, 2895–2898. [CrossRef]

31. Huang, Z.; Duan, H.; Liu, J. Preparation of lanthanum cerate powders via a simple molten salt route. *Ceram. Int.* **2016**, *42*, 10482–10486. [CrossRef]

32. Liu, X.; Antonietti, M. Molten salt activation for synthesis of porous carbon nanostructures and carbon sheets. *Carbon* **2014**, *69*, 460–466. [CrossRef]

33. Deng, X.; Zhao, B.; Zhu, L. Molten salt synthesis of nitrogen-doped carbon with hierarchical pore structures for use as high-performance electrodes in supercapacitors. *Carbon* **2015**, *93*, 48–58. [CrossRef]

34. Petnikota, S.; Maseed, H.; Srikanth, V. Experimental elucidation of a graphenothermal reduction mechanism of Fe_2O_3: An enhanced anodic behavior of an exfoliated reduced graphene oxide/Fe_3O_4 composite in Li-ion batteries. *J. Phys. Chem. C* **2017**, *121*, 3778–3789. [CrossRef]

35. Das, B.; Reddy, M.V.; Chowdari, B.V.R. Li-storage of Fe_3O_4/C composite prepared by one-step carbothermal reduction method. *J. Alloy Compd.* **2013**, *565*, 90–96. [CrossRef]

36. Li, S.; Liang, F.; Wang, J. Preparation of mono-dispersed carbonaceous spheres via hydrothermal process. *Adv. Powder Technol.* **2017**, *28*, 2648–2657. [CrossRef]

37. Tian, L.; Li, J.; Liang, F. Molten salt synthesis of tetragonal carbon nitride hollow tubes and their application for removal of pollutants from wastewater. *Appl. Catal. B Environ.* **2017**, *225*, 307–313. [CrossRef]

38. Gao, H.; Yan, S.; Wang, J. Towards efficient solar hydrogen production by intercalated carbon nitride photocatalyst. *Phys. Chem. Chem. Phys.* **2013**, *15*, 18077–18084. [CrossRef]

39. Sevilla, M.; Ferrero, G.A.; Fuertes, A.B. One-pot synthesis of biomass-based hierarchical porous carbons with a large porosity development. *Chem. Mater.* **2017**, *29*, 6900–6907. [CrossRef]

40. Ma, C.; Chen, X.; Long, D. High-surface-area and high-nitrogen-content carbon microspheres prepared by a pre-oxidation and mild KOH activation for superior supercapacitor. *Carbon* **2017**, *118*, 699–708. [CrossRef]

41. Estevez, L.; Prabhakaran, V.; Garcia, A.L. Hierarchically porous graphitic carbon with simultaneously high surface area and colossal pore volume engineered via ice templating. *ACS Nano* **2017**, *11*, 11047–11055. [CrossRef] [PubMed]

42. Wang, H.; Meng, F.; Li, J. Carbonized design of hierarchical porous carbon/Fe_3O_4@Fe derived from loofah sponge to achieve tunable high-performance microwave absorption. *ACS Sustain. Chem. Eng.* **2018**, *11*, 11801–11810. [CrossRef]

43. Li, P.; Bai, G.; Liu, T. Preparation of nano-Fe_2O_3/C supercapacitor electrode material by solution combustion method. *New Chem. Mater.* **2015**, *9*, 48–50.

44. Islam, M.A.; Ahmed, M.J.; Khanday, W.A. Mesoporous activated carbon prepared from NaOH activation of rattan (*Lacosperma secundiflorum*) hydrochar for methylene blue removal. *Ecotoxicol. Environ. Saf.* **2017**, *138*, 279–285. [CrossRef] [PubMed]

45. Tan, I.A.W.; Ahmad, A.L.; Hameed, B.H. Adsorption of basic dye on high-surface-area activated carbon prepared from coconut husk: Equilibrium, kinetic and thermodynamic studies. *J. Hazard Mater.* **2008**, *154*, 337–346. [CrossRef] [PubMed]

46. Önal, Y.; Akmil-Başar, C.; Sarıcı-Özdemir, Ç. Investigation kinetics mechanisms of adsorption malachite green onto activated carbon. *J. Hazard Mater.* **2007**, *146*, 194–203. [CrossRef] [PubMed]

47. Guo, Y.; Zhao, J.; Zhang, H. Use of rice husk-based porous carbon for adsorption of rhodamine B from aqueous solutions. *Dyes Pigment.* **2005**, *66*, 123–128. [CrossRef]

48. Chen, Z.; Yingjie, L.; Weihao, Z. Synthesis and Zn(II) modification of hierarchical porous carbon materials from petroleum pitch for effective adsorption of organic dyes. *Chemosphere* **2019**, *216*, 379–386.

49. Hao, Y.; Wang, Z.; Wang, Z. Preparation of hierarchically porous carbon from cellulose as highly efficient adsorbent for the removal of organic dyes from aqueous solutions. *Ecotoxicol. Environ. Saf.* **2019**, *168*, 298–303. [CrossRef]